In-materio computing in random networks of carbon nanotubes complexed with chemically dynamic molecules: a review

NEUROMORPHIC
Computing and Engineering

TOPICAL REVIEW

In-materio computing in random networks of carbon nanotubes complexed with chemically dynamic molecules: a review

H Tanaka[1,2,3,4,*], **S Azhari**[1,2,5], **Y Usami**[1,2], **D Banerjee**[2], **T Kotooka**[2], **O Srikimkaew**[2,3], **T-T Dang**[2,4], **S Murazoe**[2], **R Oyabu**[2], **K Kimizuka**[2] **and M Hakoshima**[2]

[1] Research Center for Neuromorphic AI Hardware, Kyushu Institute of Technology (Kyutech), 2-4 Hibikino, Wakamatsu, Kitakyushu 8080196, Japan
[2] Graduate School of Life Science and Systems Engineering, Kyushu Institute of Technology (Kyutech), Kitakyushu 8080196, Japan
[3] Institute of Science, Suranaree University of Technology, Nakhon Ratchasima 30000, Thailand
[4] Faculty of Applied Science, Ho Chi Minh University of Technology, District 10, Ho Chi Minh City, Vietnam
[5] Present address: Graduate School of Information, Production and Systems, Waseda University, Kitakyushu 8080135, Japan.
[*] Author to whom any correspondence should be addressed.

E-mail: tanaka@brain.kyutech.ac.jp

Keywords: reservoir computing, neuromorphic, neural network, deep learning, non-linearity, artificial intelligence

OPEN ACCESS

RECEIVED
6 December 2021

REVISED
31 March 2022

ACCEPTED FOR PUBLICATION
14 April 2022

PUBLISHED
20 May 2022

Abstract

The need for highly energy-efficient information processing has sparked a new age of material-based computational devices. Among these, random networks (RNWs) of carbon nanotubes (CNTs) complexed with other materials have been extensively investigated owing to their extraordinary characteristics. However, the heterogeneity of CNT research has made it quite challenging to comprehend the necessary features of *in-materio* computing in a RNW of CNTs. Herein, we systematically tackle the topic by reviewing the progress of CNT applications, from the discovery of individual CNT conduction to their recent uses in neuromorphic and unconventional (reservoir) computing. This review catalogues the extraordinary abilities of random CNT networks and their complexes used to conduct nonlinear *in-materio* computing tasks as well as classification tasks that may replace current energy-inefficient systems.

1. Introduction

With the rapid progress of software-based artificial intelligence (AI), the high energy consumption of contemporary complementary metal-oxide-semiconductor (CMOS) systems has becomes a major concern. Therefore, analog hardware-based AI techniques are required [1]. Notably, innovative analog-based phenomena derived from the material sciences present exciting new opportunities. For example, material-based composites have been found to enable signal processing, computation, and memory storage, which if configured properly, may be from 10 to 100-times more efficient, thus easing energy burdens.

This study contributes to the future development of neuromorphic AI hardware by cataloguing the intelligent capabilities inherent in random networks (RNWs) that combine nonlinearity and other properties [2–8] to mimic the dynamics of the human brain [9, 10]. This review provides a historic review of carbon nanotube (CNT) RNWs and their composites to better understand their conductive and neuromorphic properties, as illustrated in figure 1.

2. Electric nonlinearity of individual CNT and CNT complexed with molecules

At the microscopic scale, the human brain exhibits clearly nonlinear dynamics [9, 11]. To reproduce synaptic and neuromorphic properties, a combination of two nonlinear components (i.e., a CNT and molecule) is essential. For a synapse, the CNT/molecule component should be such that it resembles the nonlinear resistive switching characteristic. Such dynamics give rise to multiple resistive/conductive states, representative of biological synaptic weights, from within the network, hence making it more of a memory unit, where the states can be modified by controlling the charge influx through it via external stimulation. While, for emulating the biological neuron, energy efficient information generation, such as spike interval or density is required from a

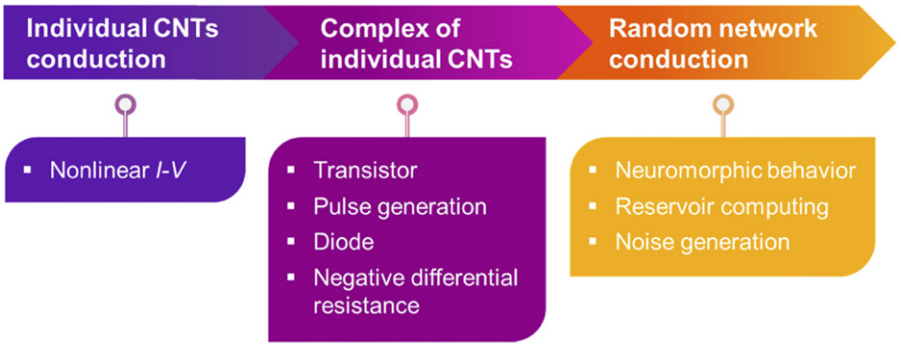

Figure 1. Lowest to highest levels of abstraction on how intelligence has emerged from CNT RNWs.

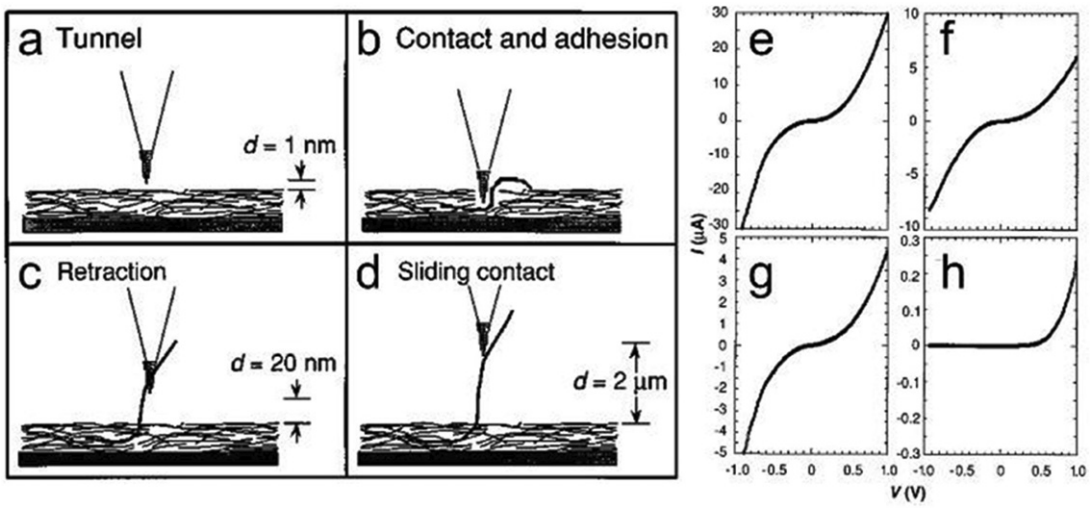

Figure 2. (a)–(d) Procedure for measuring nanotube characteristics with the tip of a single scanning tunnelling microscope. Types of current–voltage characteristics obtained for contact points at different heights of (e) 1600, (f) 1850, (g) 1950, and (h) 1980 nm along the CNT. Note the near-ideal rectification behavior in (h). (From [12]. Reprinted with permission from AAAS)

molecular functionalized CNT system. As such, the device dynamics should closely exhibit the negative differential resistance behavior in its current–voltage profile, where, after an initial non-ohmic conductance increase a rapid decrease, under the window of an increasing external stimuli, is followed. Therefore, we now examine nonlinear conduction in CNTs.

Many methods have been reported for measuring CNT electrical properties. However, the measurement of isolated CNTs was not possible until the late 1990s, when the tip of a scanning tunnelling microscope was found to induce induction and voltage (I–V) characteristics (figure 2). It was found that varying the distance between the tip and the substrate and changing CNT lengths created a variety of nonlinear I–V results that are consistent with the localized charge transport mechanism that currently allows the existence of nanoscale electronic devices [12]. Both metallic and non-metallic behaviors have been observed, along with abrupt jumps in conductivity via temperature variances [13]. This report is the earliest case of CNTs having been confirmed to exhibit nonlinear conduction without substrate interference.

Nonlinear conduction in field-effect transistors (FETs) has also been investigated. In 1998, an FET based on isolated semiconducting CNTs was fabricated and electrically measured using gate bias voltage to alter the shape of the source-drain I–V curve [14]. Tunnelling thin-film transistors (TFTs) have also emerged as potential candidates for replacing low-voltage CMOS FETs. A triple-gate CNT TFT FET, fabricated by introducing a sharp n–i–p doping profile via electrostatic doping, demonstrated a subthreshold swing (SS) of sub-60 mV/decade in a band-to-band tunnelling operation. The operation mechanism was found to overcome the fundamental SS limit of 60 mV/decade at room temperature. The nonlinear output characteristics observed in TFET operations indicate that one-dimensional CNTs are the optimal channel material for overcoming drain-induced barrier thinning by operating within the quantum capacitance limit [15].

Some nanoparticle (NP)-based CNT complexes have been found to show specific electrical properties from the combination of CNTs and adsorbed NP molecules [16]. One approach for obtaining electrical nonlinearity

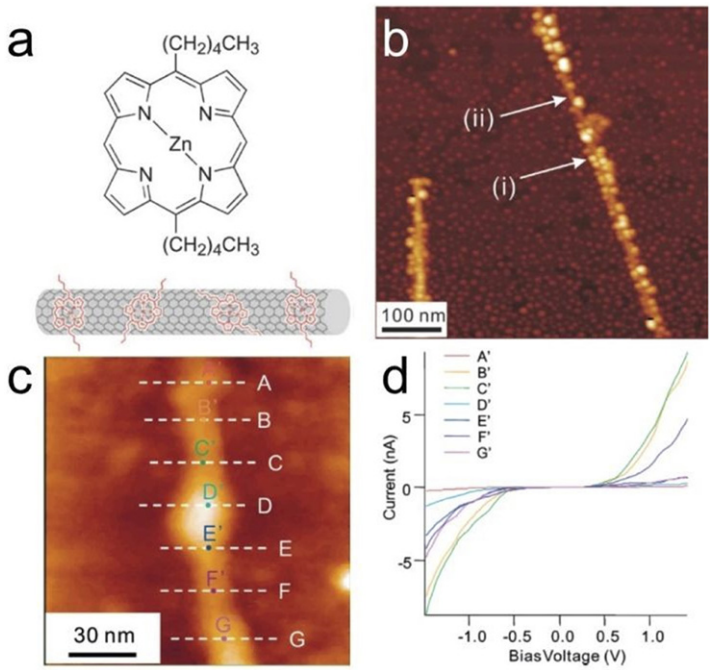

Figure 3. (a) Structural formula of synthesized 5,15-bispentylporphyrinato zinc(II) (BPP-Zn) and the SWNT/BPP-Zn complex. (b) Tapping-mode AFM image of BPP-Zn on an SWNT electrode. The SWNT is almost entirely covered by BPP-Zn aggregates, as indicated by arrow (i). Some sections of the SWNT are partially exposed, as indicated by the arrow (ii). (c) Topographic image of BPP-Zn absorbed on an SWNT electrode. I–V measurements are carried out at points A′–G′. (d) I–V curves obtained at each point. ([17] John Wiley & Sons. Copyright © 2006 WILEY-VCH Verlag GmbH & Co. KGaA, Weinheim)

is to complement NP materials with CNTs for electrical functionalization. Many types of materials have been reported to support this. For instance, Tanaka *et al* reported the adsorption of 5,15-bispentylporphyrinato zinc(II) (BPP-Zn) NPs on the sidewalls of single-walled nanotubes for electrical functionalization, as shown in figures 3(a) and (b). Point contact current imaging atomic force microscopy (AFM) was used to measure the I–V curves, which showed nonlinear electrical properties as a result of the NPs behaving as nanodiodes on the single-wall nanotube (SWNT) wiring [17]. Another report suggested that a porphyrin single molecule can operate as a point local gate for individual SWNT FETs owing to the redox of a single molecule [18], which can be a source of telegraph noise of the system.

Similar studies using a 150mer-porphyrin polymer (150mer-porph) also reported enhanced conductivity of SWNTs owing to the π electron donation from the 150mer-porph [19]. Conductivity measurements with metallic nanotubes isolated from pristine SWNTs showed that SWNTs become semiconducting in the presence of metal NPs [20]. This was further expanded to SWNT-adsorbed phosphomolybdic acid ($PMo_{12}O^{-40}$; POM), which results in an SWNT/POM junction in which rectification direction inversion arises from SWNT particle size or chirality. Kelvin probe force microscopy measurements showed that the charge distribution of POM/semiconducting SWNTs was opposite to that of POM/metallic SWNTs [21].

Other CNT-based CMOS approaches exist. For example, a CMOS-like inverter was integrated using ambipolar CNT transistors. The ambipolarity of Schottky-barrier CNT FETs is a well-known phenomenon that occurs in a vacuum environment or with a top-gate oxide and electrode. A new approach that considers beneficial ambipolarity in a CNT-based CMOS circuit was proposed in which CMOS-like logic circuits (e.g., inverters and NOR/NAND gates) lacking an unreliable doping process were integrated using ambipolar CNT transistors (figure 4) that automatically configured themselves to act as n- or p-type logic gates, depending on the exchange of supply voltage (V_{DD}) and ground [22].

Figure 5 also shows SWNT-based CMOS logic circuits with sub-nanowatt static power consumption through the threshold voltage tuning of constituent p- and n-type SWNT transistors [23]. This behavior is enabled by a local metal gate structure that achieves enhancement-mode p- and n-type SWNT TFTs with widely separated and symmetric threshold voltages. These complementary SWNT TFTs are reported to demonstrate a CMOS inverter and NAND and NOR logic gates at supply voltages as low as 0.8 V with an ideal rail-to-rail operation, sub-nanowatt static power consumption, high gain, and excellent noise immunity. This is accomplished by precisely tuning the p- and n-type TFT threshold voltages to match the ideal conditions for an integrated CMOS device. The resulting logic gates exhibit symmetric rail-to-rail operation and excellent noise immunity, allowing the use of cascaded multiple logic gates in highly integrated circuits.

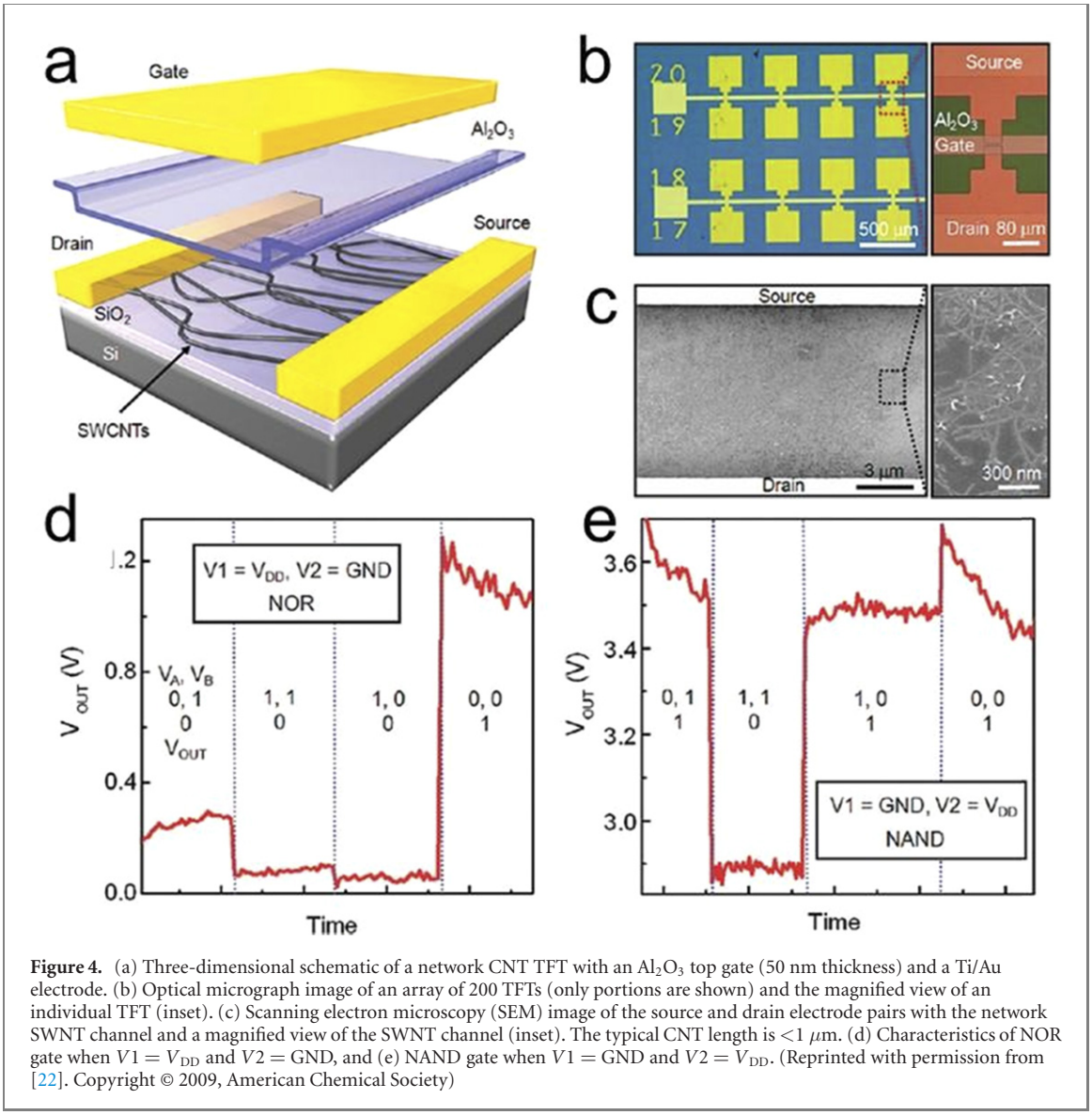

Figure 4. (a) Three-dimensional schematic of a network CNT TFT with an Al_2O_3 top gate (50 nm thickness) and a Ti/Au electrode. (b) Optical micrograph image of an array of 200 TFTs (only portions are shown) and the magnified view of an individual TFT (inset). (c) Scanning electron microscopy (SEM) image of the source and drain electrode pairs with the network SWNT channel and a magnified view of the SWNT channel (inset). The typical CNT length is <1 μm. (d) Characteristics of NOR gate when $V1 = V_{DD}$ and $V2 =$ GND, and (e) NAND gate when $V1 =$ GND and $V2 = V_{DD}$. (Reprinted with permission from [22]. Copyright © 2009, American Chemical Society)

Reports suggest that the adsorption of molecules on CNTs can control their electrical properties. Similarly, CNT electrical properties can be controlled by exposing them to chemical analytes (e.g., ethanol, benzene, acetone, and toluene) for functionalization. As shown in figure 6, reversible nonlinear I–V characteristics with higher-than-usual resistance and suppressed zero-bias conductance depend on the chemical analyte. For example, when the chemical analytes interact with the CNT surface, conductivity decreases. These results confirm the chemical selectivity of CNTs and their electrical interactions with different chemical analytes [24].

Another way to generate nonlinearity may be to selectively dope the channels of SWNT networks with triethyl oxonium hexachloroantimonate and polyethylenimine to form p–i–n junctions with strong built-in electric fields. Using this method, high-performance diodes with a high rectification ratio, large forward current, and low reverse saturation current have been realized [25], and the I–V characteristics show clear nonlinear rectifying properties. An asymmetric contact was found to effectively improve p–i–n diode performance [26]. A three-dimensional electrolyte-accessible electrode structure was developed to achieve a high-performance rate in an organic electrolyte. Additionally, $Ti_3C_2T_x$-based specially synthesized knotted CNTs, as shown in figure 7, were used to support a Ti_3C_2 network. The electrode structure was modified to simultaneously maximize ion accessibility and minimize the tortuosity of the ion transport pathways. MXene-knotted CNT composite electrodes have been reported to exhibit high capacitance with a scan rate of more than three orders of magnitude [27].

Another interesting report suggested the direct production of a CNT composite via the fermentation of yeast extract in the presence of CNT aqueous dispersion. Electrical and optical analyses demonstrated that the fermentation of beer yeast in the presence of CNTs enhanced nonlinearity, electrical conductivity, and photoconductive activity of the composite film [28].

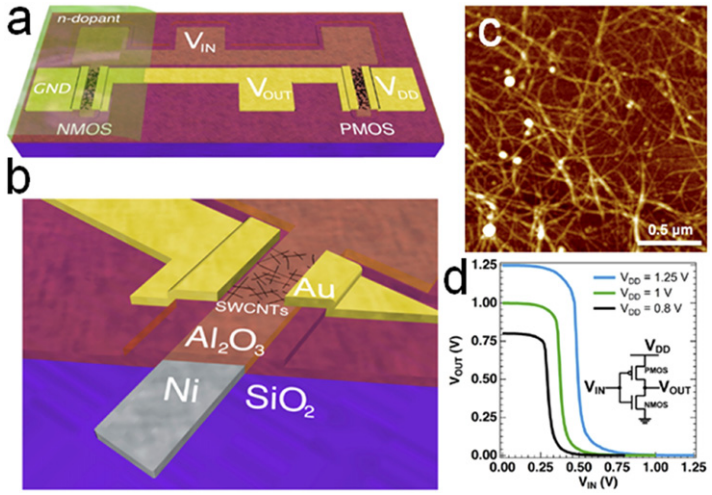

Figure 5. SWNT CMOS device structure. (a) SWNT CMOS inverter, including the unencapsulated p-type TFT and benzyl viologen-doped n-type TFT. (b) Cross-section of an individual SWNT TFT consisting of SiO_2 on a Si substrate, a local Ni gate, deposited Al_2O_3 layer, >99% pure deposited semiconducting SWNTs, and Cr/Au source/drain contacts. (c) AFM image of the SWNT film morphology within the TFT channel region. (d) SWCNT CMOS inverter electrical characteristics. Voltage transfer curves for $V_{DD} = 0.8$, 1, and 1.25 V (inset shows the circuit diagram of the inverter). (Reprinted with permission from [23]. Copyright © 2013, American Chemical Society)

In summary, the nonlinearity of CNT RNWs and their performance characteristics provide all the necessary properties for *in-materio* computing. In the following sections, we explain how this can be used for neuromorphic computing.

3. Neuromorphic devices and hardware on a random network of CNTs

Independent of AI, neuromorphic hardware has emerged as its own research field that focuses on neuroscience, wherein the construction of spiking neurons and their dense, complex networks is the first step of *in-materio* and in-memory computing. However, the integration density of current neuromorphic devices is much lower than that of the human brain.

A molecular neuromorphic device comprising a dynamic and extremely dense RNW of SWNTs complexed with POM [29] was experimentally shown to generate spontaneous spikes and noise. The authors proposed an electron-cascading model consisting of heterogeneous molecular junctions that yielded results in good agreement with theory, indicating the possibility that complex functional networks could be constructed using molecular devices (figure 8).

Another approach to fabricating synaptic tendencies involves optically gated (OG) CNT FET-based synapses (figure 9) [30]. The device is controlled by light irradiation, and conductance is programmed by applying electrical pulses. A neuromorphic computing architecture was proposed using the principal advantage of the gate protection effect based on a crossbar geometry in which the gate electrodes are shared in the same row. The crossbar architecture is believed to learn several functions in a massively parallel manner while promising high reliability, high density, and fast learning.

CNT synaptic transistors have also been fabricated from a hydrogen-doped PEG electrolyte sandwiched between the CNT channel and a Ti/Al top-gate electrode (figure 10) [31]. The CNT synapse was operated based on the dynamic interactions between the CNTs and hydrogen ions in an electrochemical cell (key to synaptic mechanisms). Under spike stimulation, the device emulates the dynamic logic, learning, and memory functions of a biological synapse with low energy consumption.

Although the CNT synapse has an FET structure, an oxide dielectric layer was later implanted with indium ions as the gate instead of integrating the hydrogen-doped PEG electrolyte [32]. To imitate the dynamic functions of a neuron and an axon, a CNT-based FET and a Si-based integrate-and-fire (I & F) circuit were used. By applying input spikes and using the I & F circuit to trigger output spikes, dynamic analogue post-synaptic currents and an excitatory post-synaptic current (EPSC) and inhibitory post-synaptic current (IPSC) were successfully emulated (figure 11).

In another report, an FET structure was developed to improve the capability of CNT synapses. Half of the CNT channel was converted using aluminium oxide (Al_2O_3) film, changing the CNTs from p- to n-types. As a result, a p–n junction was formed in the CNT channel, and the Schottky barrier increased between the n-type CNTs and their metal contacts. Thus, the baseline current through the CNT channel in an idle state was

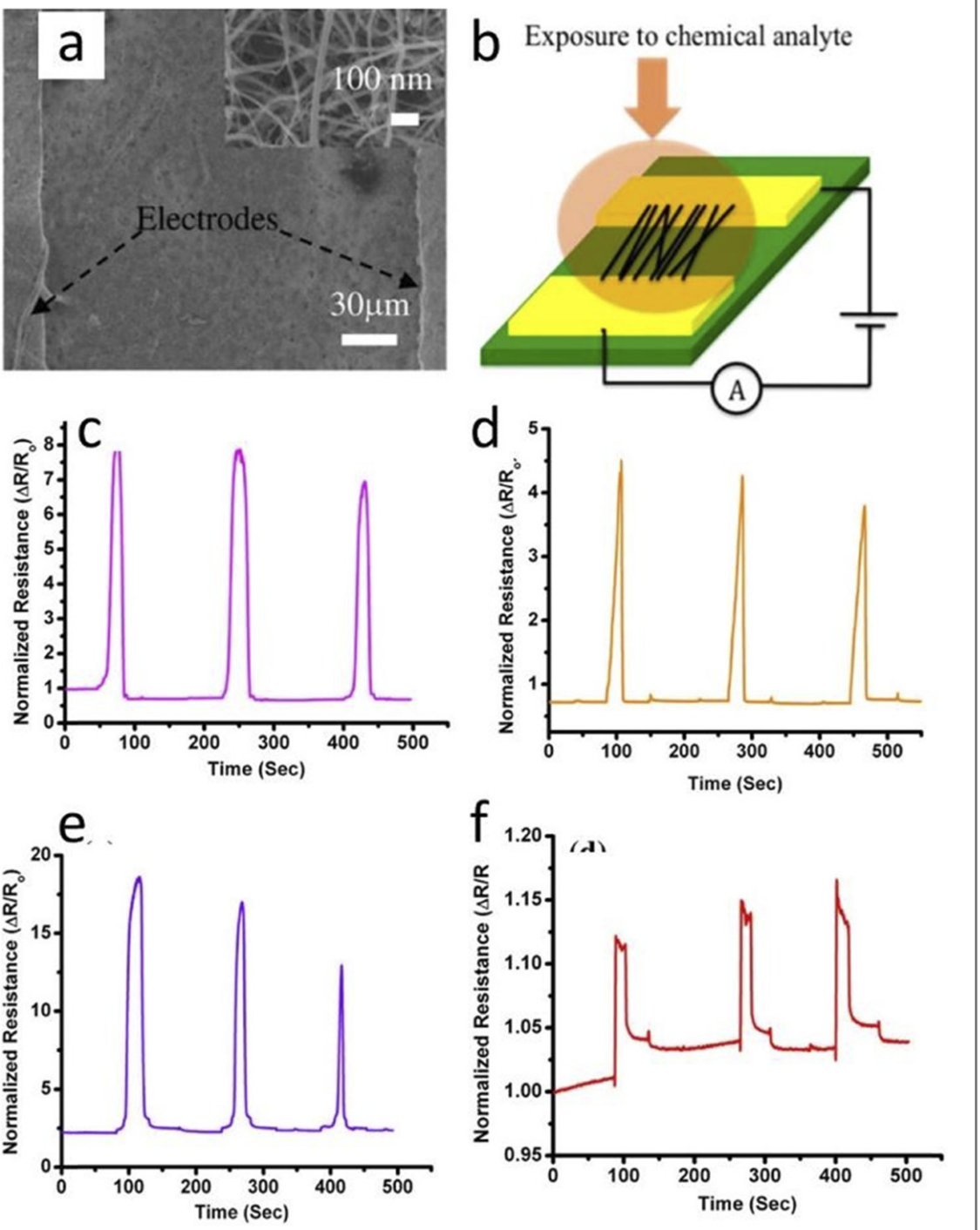

Figure 6. (a) Scanning electron microscopy image of CNT dispersed gold electrodes used for sensing organic analytes. The inset shows the microstructure of a CNT mat between electrodes. (b) Experimental setup used for the CNT sensor. (c)–(f) Cyclic response shown for the CNT samples with different analytes: (c) toluene, (d) benzene, (e) ethanol, and (f) acetone. (Reproduced from [24].)

significantly reduced, thus improving power efficiency. Excitatory and inhibitory synapses were emulated using multiple CNT synapses integrated with a Si-based soma circuit [33]. Additionally, a light-stimulated neuromorphic device made of printed photogate SWNT TFT-based synapses was reported. In such devices, the synaptic mechanism is induced by photogenerated carriers and trapping states in the interfaces. Under pulsed light stimulation, synaptic functions (e.g., learning, memory, and signal filtering) are successfully emulated. Multimodal optoelectronic SWNTs mixed with lead-free perovskite ($CsBi_3I_{10}$) TFTs have also been proposed. In this case, both electrical and optical pulse signals can be used together to modulate the drain currents; key synaptic functions were demonstrated. Notably, multiple artificial synapses, flash memory, and logic operations can be integrated into a single transistor. The SWNT/$CsBi_3I_{10}$ TFT successfully implemented cognitive behaviors using Pavlov's conditioning experiment and applied the recognition of handwritten digits [34].

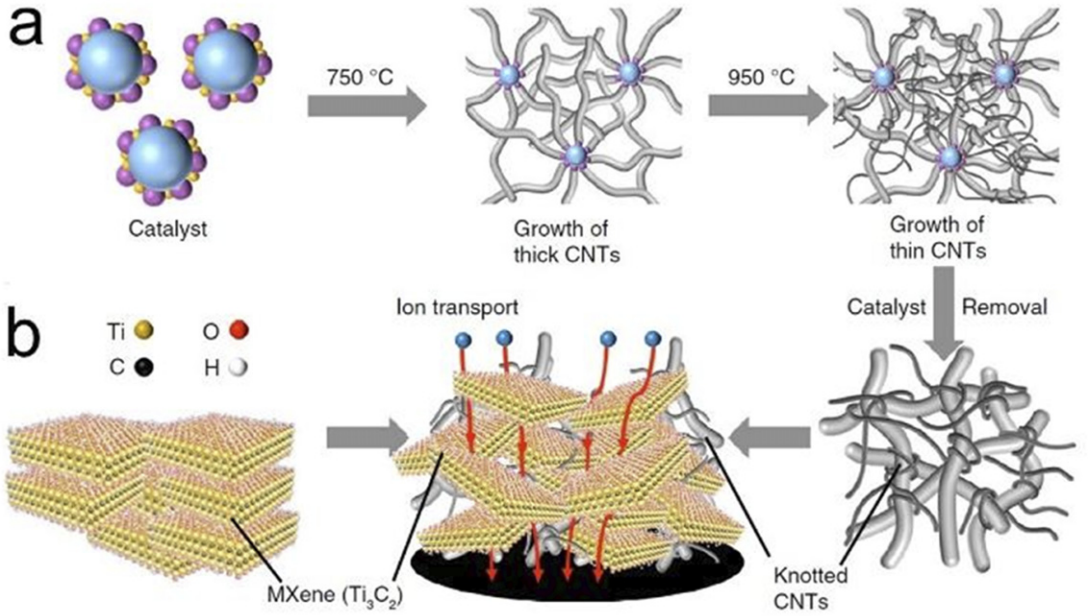

Figure 7. Design of MXene-knotted CNT composite electrodes for efficient ion transportation. (a) Synthesis process of knotted CNTs, where thin CNTs are intertwined with thicker ones. (b) MXene-knotted CNT composite electrode with reduced horizontal orientation and lower ion transport tortuosity through the electrode bulk (Reproduced from [27] CC BY 4.0.)

A novel photoneuromorphic device based on printed photogating SWNT-TFTs using lightly n-doped Si as the gate electrode was reported as similar system to the learning and memory functions of brain-inspired neuromorphic systems [35].

Poly(vinyl alcohol) (PVA) was used as the dielectric layer in a biocompatible synaptic transistor [36]. A flexible (F) transparent CNT synaptic transistor (ST)—based synapse was proposed. The behaviors of biological synapses, including spike-dependent plasticity, paired-pulse facilitation, and short- and long-term plasticity, were emulated. The F-CNT-STs exhibited high flexibility and their synaptic functions remained functional after 1000 bending cycles (figure 12).

In another fabrication approach, flexible printed SWNT TFTs using solid-state electrolyte dielectrics composed of a mixture of ion liquids and cross-linked poly(4-vinylphenol) were used as dielectric layers [37]. These devices can simulate basic synaptic plasticity such as EPSC and paired-pulse facilitation, as well as their inhibitory characteristics. It exhibits good stability and mechanical flexibility, and the change in the EPSC curve is almost negligible before, during, and after bending (figure 13).

A CNT transistor was used to demonstrate an artificial tactile sensor system [38], exhibiting a semi-volatile characteristic that can switch the operation mode (volatile or nonvolatile) according to the bias condition. As a semi-volatile device, both sensory neurons and the perceptual synaptic network were implemented as a single device. The tactile sensor system distinguishes temporally correlated pressure stimuli and extracts features of the tactile patterns for pattern recognition (figure 14).

A unique study on neuromorphic devices was later conducted through which more attention was paid toward utilizing biocompatible and biodegradable materials [39]. A degradable chlorophyll-a/SWNT synaptic transistor was developed on a PVA substrate to provide a naturally biodegradable and water-soluble device to demonstrate zero e-waste (figure 15). Key synaptic functions, including EPSC, paired-pulse facilitation, transition from short- to long-term memory, and learning and forgetting experiences, were successfully realized with this device. The device dissolved with rainfall and completely decomposed after 5 min.

4. *In-materio* physical reservoir computing (RC) devices on CNT random network

Hereafter, we describe reservoir computing (RC) devices based on material engineering. Several approaches have been developed to complement current AI hardware with material devices. An artificial neural network (ANN) inspired by the biological neuromorphic behavior of the brain is shown in figure 16(a). Most current AI systems comprise feedforward-propagating neural networks (NNs). Each node computes a nonlinear transformation of the sum of the products between the incoming signals and their synaptic weights, plus an additional bias term (red circles in figure 16(a)). When this kind of system contains more than three hidden (middle) layers, it qualifies as deep learning [40]. Unlike feed-forward propagation NNs, recurrent NNs (RNNs) can

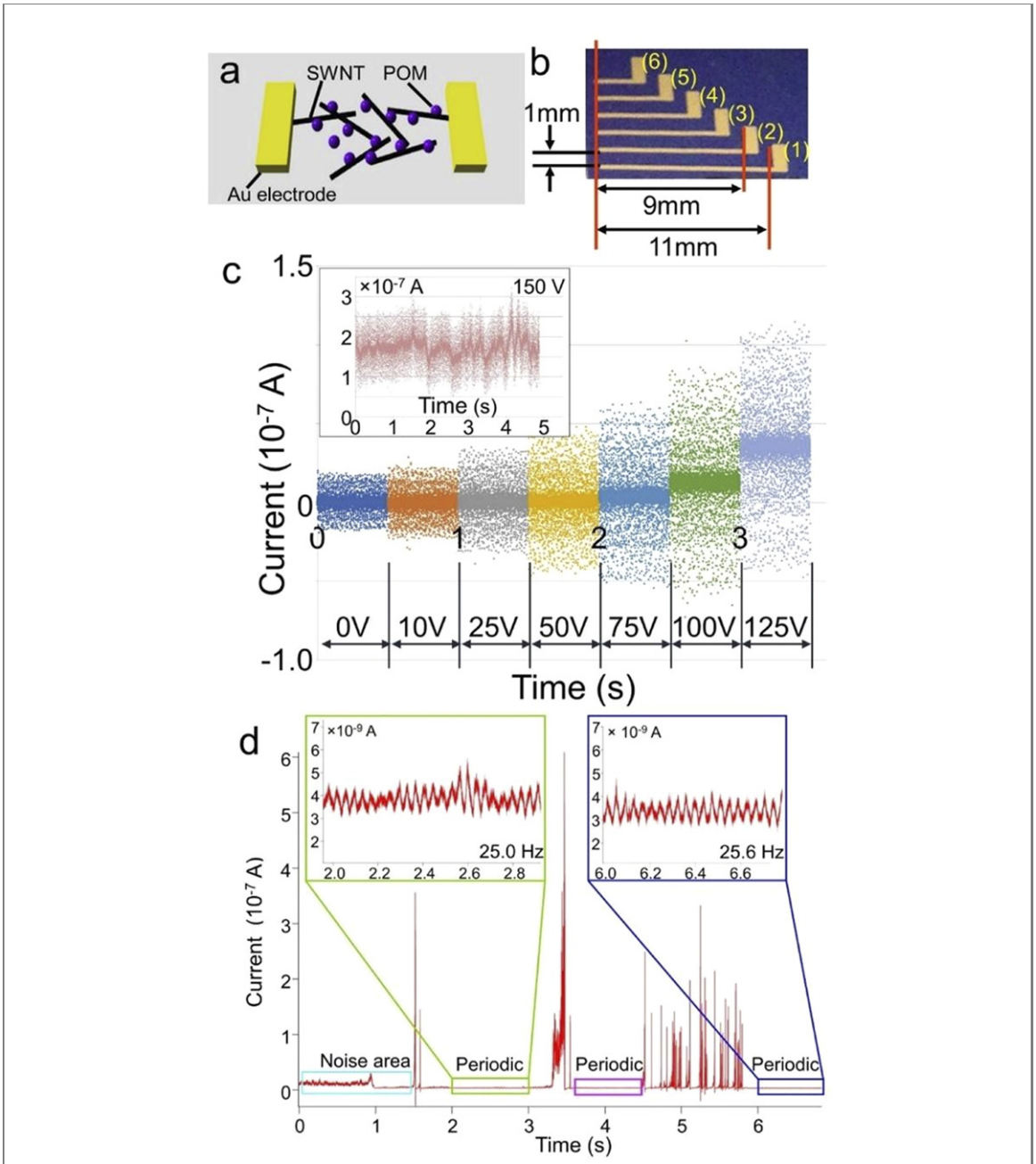

Figure 8. Experimental setup and noise generation of a SWNT phosphomolybdic acid (POM) network. (a) SWNT/POM complex network. Yellow cuboids, black tubes, and purple spheres represent terminal electrodes, SWNTs, and POM particles, respectively. (b) Substrate covered with the SWNT/POM complex that includes six electrodes. (c) Sampled current density over time, representing current magnitude distributions with the bias voltage increasing stepwise across electrodes from 0 to 125 V for the network. (Inset) Current becomes unstable at 150 V. (d) Time dependence of the current under humidity. (Inset) Magnification of periodic base current modulation. (Reproduced from [29] CC BY 4.0.)

use their internal state (memory) to process any sequence of inputs, meaning that some information from a given node can be fed back into the original, as shown by the blue circle arrows in figure 16(a). This allows them to exhibit temporal dynamics [41] suitable for tasks such as non-segmented, connected handwriting [42] and speech recognition [43, 44]. RC is a special RNN case, as shown in figure 16(b); it was developed from echo-state networks (ESNs) [45, 46] and liquid-state machines [47] as its information-processing framework [48, 49]. The ESN provides an architecture and a supervised learning principle for RNNs for the RC system, in which the hidden layer is treated as a black box, indicating that the internal weight of the network is fixed. Strong nonlinearity, high dimensionality, and higher memory are necessary properties of an RC system. Learning is conducted only in the output layer through simple linear regression. The *in-materio* and physical RC is reported to be in good agreement with RC theory. Hence, there have been many interesting reports about the materials needed to develop RC devices.

The high-dimensional nonlinear transformation of the input signals obtained as a function of the output signals can be treated equivalently to the information generated when a software-designed NN architecture

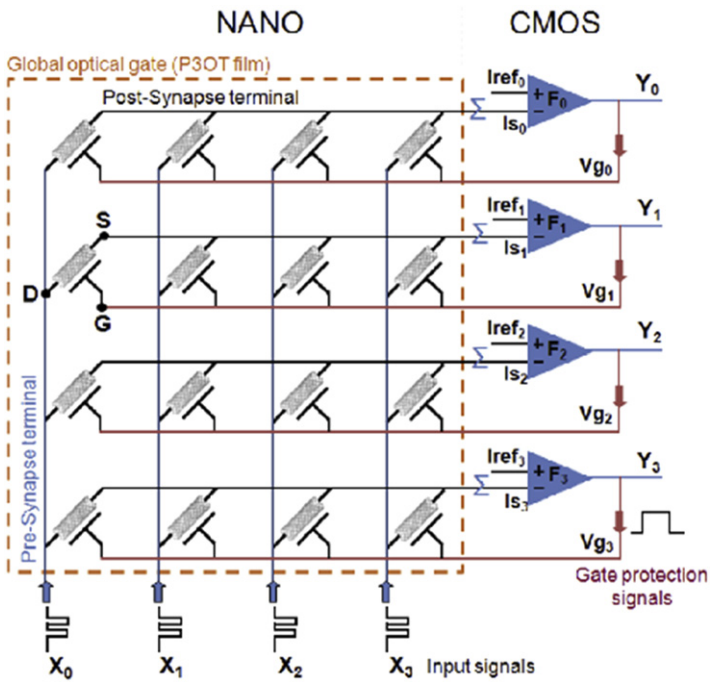

Figure 9. Crossbar architecture comprising four neurons (CMOS-based) and 16 synapses (OG CNT FETs). Each neuron is associated with four synapses within a row that share the same electrical gate (Vg_i) and source terminal. The drain terminals (vertical pre-synapse) connect the synapses from different neurons and apply programming pulses during learning and input signals during computing. All synapses in the array share a common P3OT film OG terminal. The output of the functions (Y_i) and the feedback signals to the gate (Vg_i) are produced through simple CMOS based neurons. (Reproduced from [30], with permission from Springer Nature.)

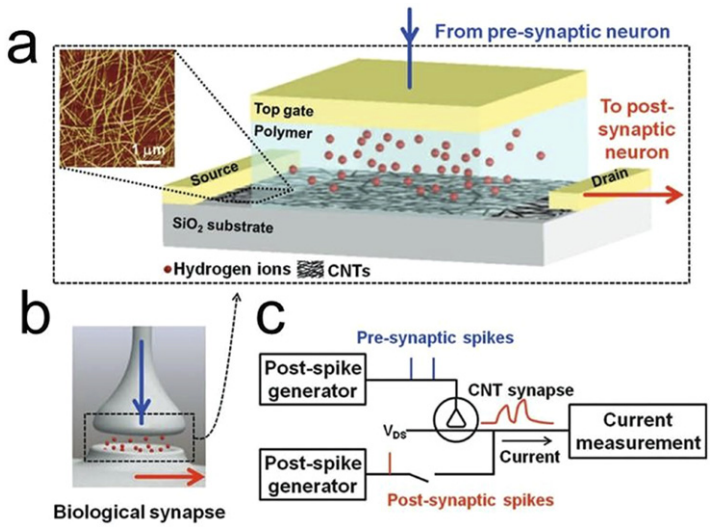

Figure 10. Structure of a CNT synapse and a post-synaptic current triggered by a pre-synaptic spike. (a) The transistor-like structure of a CNT synapse is shown with an electrochemical cell containing hydrogen ions in a polymer electrolyte integrated into its gate. The inset shows an AFM image of a random CNT network and the average density of the single-wall CNT. (b) Biological synapse between pre- and post-synaptic neurons. (c) A symbol representing the CNT synapse within a scheme showing that a pre-synaptic potential spike applied on its top gate triggers an excitatory post-synaptic current on its drain. ([31] John Wiley & Sons. Copyright © 2013 WILEY-VCH Verlag GmbH & Co. KGaA, Weinheim.)

operates with a nonlinear activation function. Therefore, hardware can be implemented by simply learning these output signals without the need for a separate information processor. Although many such hardware NN models [50] have been studied, RC is novel and has only recently attracted significant attention (figure 16(b)) [51–54] owing to its straightforward framework for processing time-series data. The execution of RC learning for time-series prediction tasks has been applied to atomic switch networks (ASNs) [55–57], memristor networks [58], CNT/polymer composites [59, 60], NP aggregation [57], polymer network systems [61],

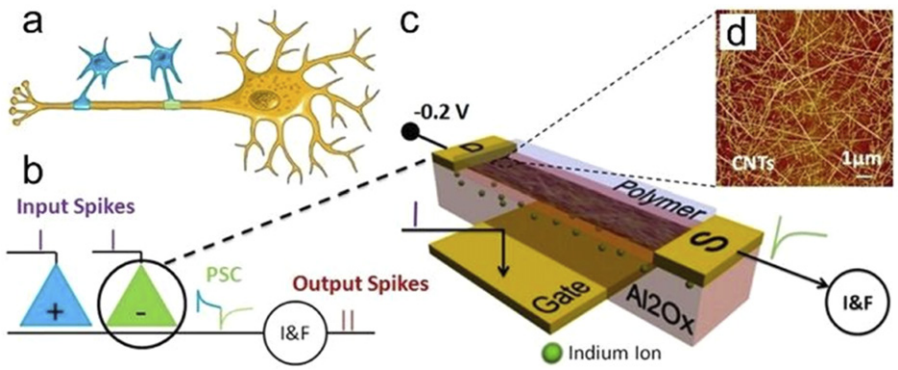

Figure 11. (a) Scheme showing a neuron (yellow) connected to two other neurons (blue) through synapses. (b) Structure of the neuromorphic module composed of an I & F axon circuit and synapses. Input spikes induce an EPSC through an excitatory CNT synapse (blue '+' triangle) and an IPSC through an inhibitory CNT synapse (green '–' triangle). Dynamic PSCs flow jointly toward the I & F circuit and trigger output spikes. (c) CNT synapse with a channel composed of a random CNT network connected with source (S) and drain (D) electrodes. Indium ions are implanted into an aluminum oxide dielectric layer in the transistor gate. A potential of $V_{ds} = -0.2$ V is applied to an inhibitory CNT synapse. An input spike applied to the transistor gate induces a dynamic current through the transistor channel as a PSC flows from the transistor source toward the I & F circuit. (d) AFM image of a random CNT network in the transistor channel. (Reprinted with permission from [32]. Copyright © 2013, American Chemical Society.)

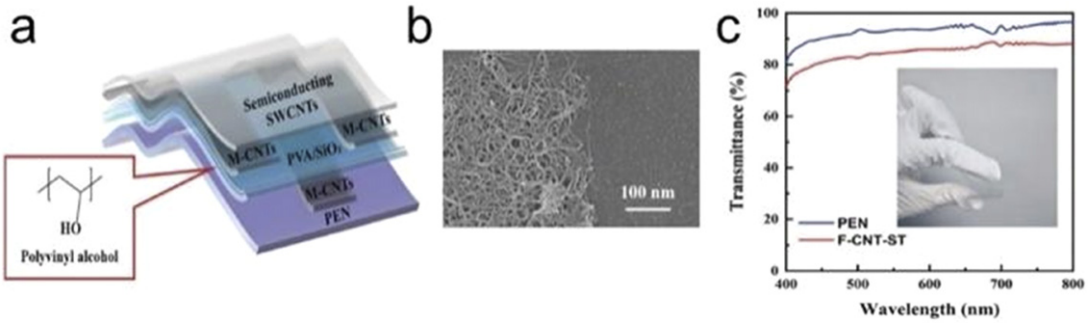

Figure 12. Characterization studies of flexible carbon nanotube synaptic transistors (F-CNT-STs). (a) F-CNT-ST illustration. (b) Scanning electron microscopy image of the electrode and channel of a representative F-CNT-ST. (c) Optical transmittance of a bare polyethylene naphthalate substrate and fabricated F-CNT-STs. (Inset) F-CNT-ST photograph. (Reproduced from [36] with permission from the Royal Society of Chemistry.)

optoelectronic systems [62, 63], soft bodies [64, 65], spintronics [4, 66], and water-tank systems [67]. The efficacy of each RC material is derived from the intrinsic reservoir property [53, 54] of recurrent nonlinear high-dimensional dynamics analogous to the human brain [10]. Irrespective of their material and fabrication diversity, their inherent dynamical complexity enables an easy input-driven computation of RC tasks with only readout trainability. Among the many physical systems, RCs with ASNs and CNTs have a promising future as large-scale bioinspired computers owing to their brain-like physicality and solution-processable RNW integration. Therefore, materials with such dynamics and physical architectures are being explored, including random SWNT networks with porphyrin POM [29].

As shown in figure 8, SWNTs are a source of noise and when functionalized with redox-active POM, they can undergo changes in their conductive states, generating brain-like random fluctuations and neuronal spike-like signals [29]. Utilizing intrinsic dynamics, an RNW structure was simulated and rudimentary learning ability through external feedback was illustrated with a theoretical RC model (figure 17(a)). Complex nonlinear dynamics were chosen from randomly selected POM molecules within the network, specifically from the source/drain side and FORCE (algorithm) learning was applied to optimize output weights to carry out the RC benchmark task of nonlinear autoregressive moving average (NARMA)-10 time-series prediction (figures 17(b)–(d)). Task learning was inferred by evaluating the normalized root mean-square deviation (NRMSD), where the lowest NRMSD implies the best optimization [30].

As an extension work of reference [29], reservoir performance of SWNT/POM was experimentally evaluated [68]. SWNT/POM with a polybutylmethacrylate (PBMA) composite was used to experimentally verify the RC task using NARMA-10. Thin composite films were prepared by ultrasonically mixing SWNTs, POM, and PBMA and drop-casting them onto a 10 × 10 grid microelectrode array. A laboratory-built experimental computing platform was designed to benchmark the supervised NARMA-10 time-series prediction. By

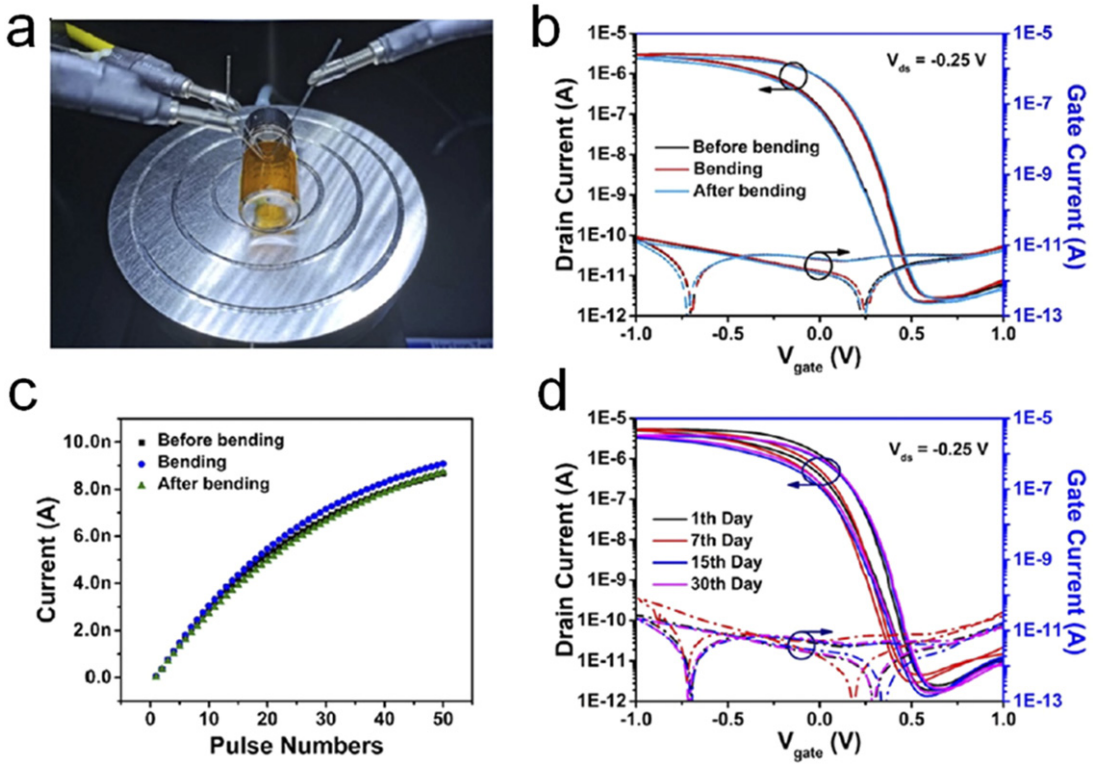

Figure 13. Stability of the flexible fully solution processed SWNT synaptic device stored under a relative humidity of 20%. (a) Flexible SWNT TFT arrays on polyimide substrate bent over a bottle with a radius of 9 mm. (b) and (c) Transfer characteristics and EPSC, respectively, of flexible device before, during, and after bending. The frequency and voltage of the stimulus sequence consisting of 50 continuous electrical pulses is 12.5 Hz and varies from 1 to 0 V, respectively. (d) Transfer curves of SWNT TFTs across 30 days. (Reproduced from [37]. © IOP Publishing Ltd. All rights reserved.)

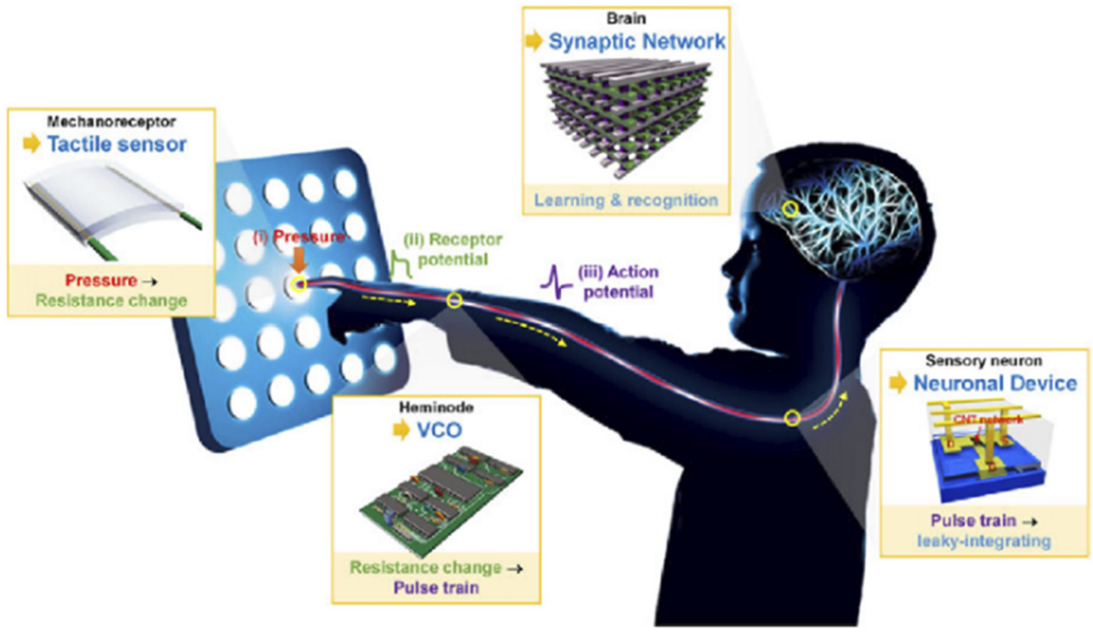

Figure 14. Conceptual design of a tactile sensor system compared with a biological sensor system. In biological systems, pressure stimuli applied to mechanoreceptors change the receptor potential of each mechanoreceptor. The receptor potentials then initiate action potentials. Action potentials from multiple nerve fibers are combined via neurons and contribute to information processing. Finally, the synaptic network in the brain recognizes the input pressure pattern. The artificial tactile sensory system comprises a tactile sensor device, voltage-controlled oscillator, neuronal device, and synaptic network. (Reproduced from [38] CC BY 4.0.)

utilizing the nonlinear current dynamics of SWNT/POM, NARMA-10 was successfully implemented with a normalized root mean-square error of 0.08, compared with the 0.19 score of the SWNT reservoir alone [69].

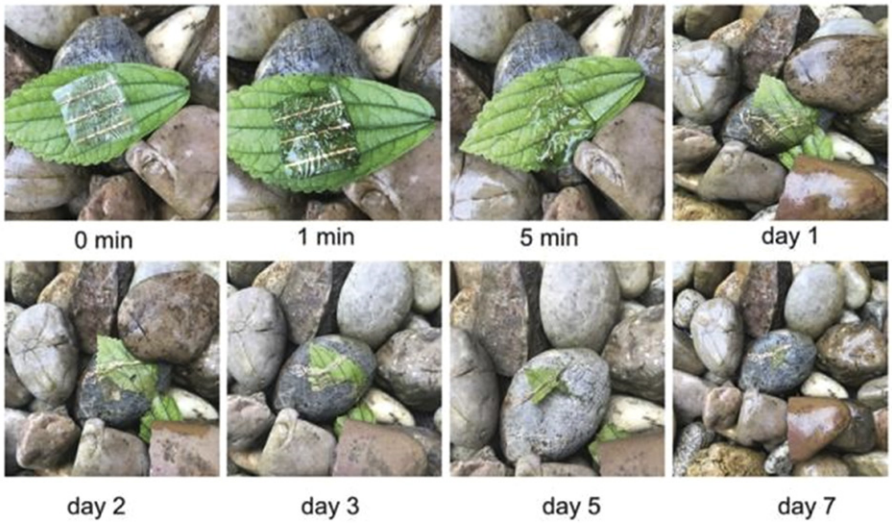

Figure 15. Demonstration of the degradable process of chlorophyll-a SWNT composite transistor array. ([39] John Wiley & Sons. © 2021 Wiley-VCH GmbH.)

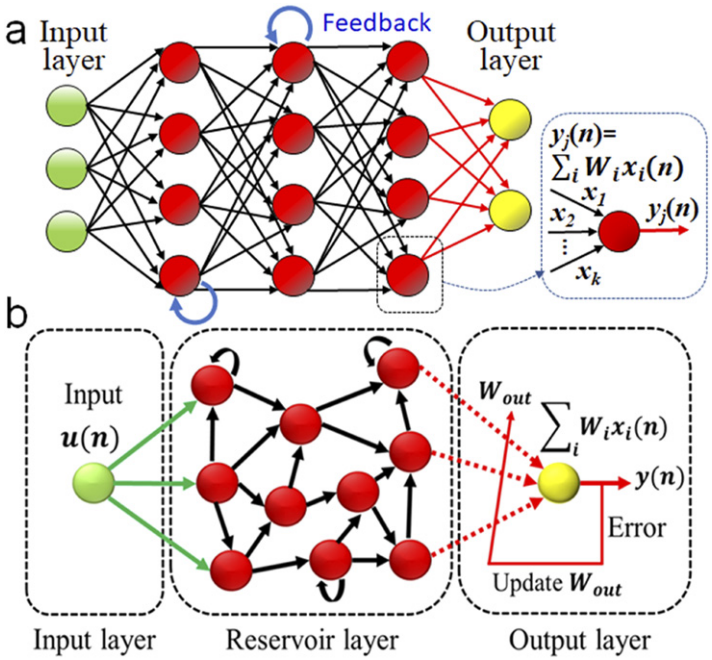

Figure 16. (a) An ANN. A recurrent take NN allows for the feedback of information (blue circle arrow) at the nodes (red circles). When signal has feedback at the nodes, the system is called as RNN. (Inset) The sum of products for all incoming signals are calculated at all nodes. (b) Reservoir network which is a kind of RNN. All nodes having non-linearity are connected randomly. Calculations in the middle layer are not required by treated as a black box. Learning is achieved only at the output layer.

In another report, a composite SWNT polymethyl methacrylate (PMMA) was used to construct an RC device using a micro-electrode array architecture (figure 18(a)) integrated into a Mecobo hardware platform consisting of field-programmable gate array-driven input/output controllers used to evolve the voltage outputs (figure 18(b)). Mecobo hardware was also interfaced with an evolutionary algorithm (EA), a genotype-based biological model that optimizes the output electrode response for a tone discriminator RC benchmark task. Generally, in a tone discriminator, two inputs of different frequencies are classified by two output classes labeled '1' for low-frequency input and '2' for high-frequency input. The RC operation was performed in real-time, and apart from the inputs and outputs, specific voltages were applied to the rest of the electrode pads used to configure the device behavior. The configuration voltages affect the electrical behavior of the CNT-polymer material, and the interaction induces certain voltages on the output electrode. The output was optimized with EA through a fitness score, where the highest score implies valid output class optimization for discriminating the input frequency tone [59].

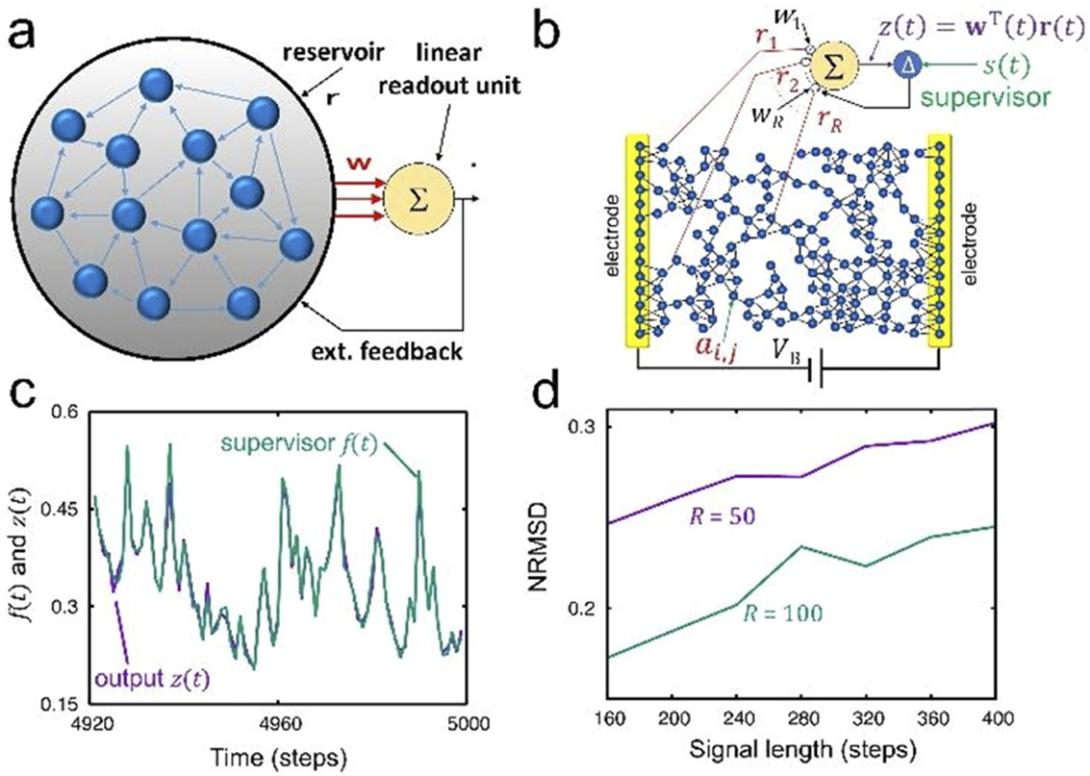

Figure 17. Demonstration of RC on the phosphomolybdic acid (POM) SWNT network (a) Illustration of a standard reservoir system with external feedback, consisting of a recurrent generator network (blue spheres and directed arrows) with firing rates r, a linear readout unit, Σ, with output z through weights w (red); output z is fed back to the reservoir. (b) Reservoir system consisting of a two-dimensional RNW of POM particles (blue spheres) sandwiched between two electrodes (yellow bars). The charge of a POM particle positioned at (i, j) is represented by $a_{i,j}$. The weight, w, is modified by the output, $z(t)$, and supervisor, $s(t)$, during the learning phase to attain $z(t) \approx s(t)$. (c) Time courses of NARMA-10 benchmark sequence, $s(t)$ (supervisor), used during FORCE learning and the output of the readout unit, $z(t)$, after learning. (d) NRMSD vs R2 (50, purple; 100, green) and the signal length from 160 to 400 steps. (Reproduced from [29] CC BY 4.0.)

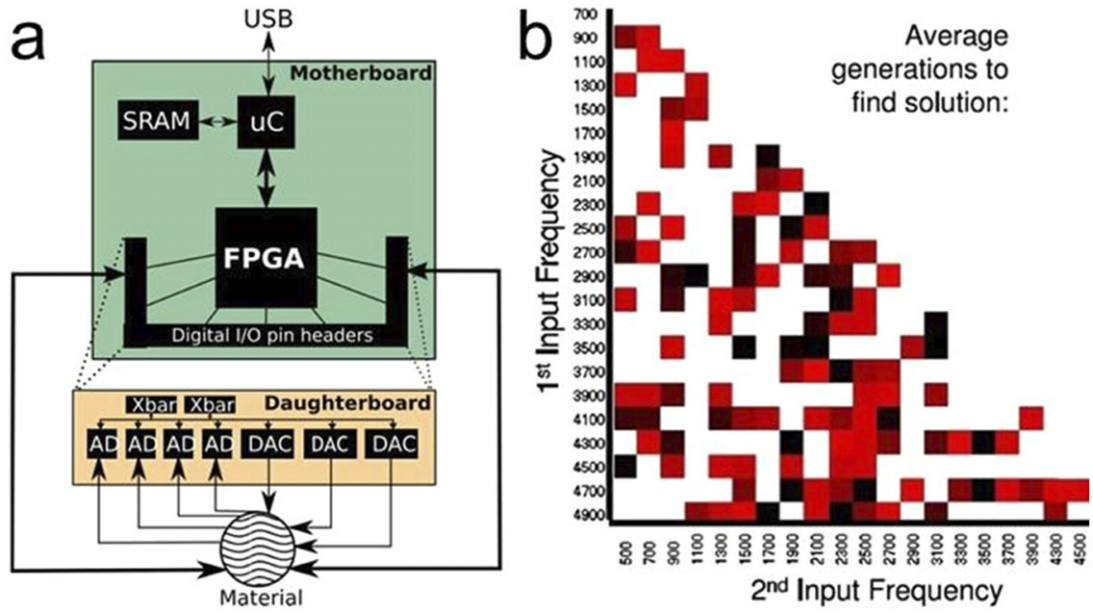

Figure 18. Demonstration of a RNW model SWNT poly(methyl methacrylate) for a tone discriminator using an EA [58] with a single 12-electrode array (circular) and one material sample. (a) Mecobo hardware interface implementation overview. (b) Tone discriminator results for 114 pairs of frequencies. (Reproduced from [59], with permission from Springer Nature.)

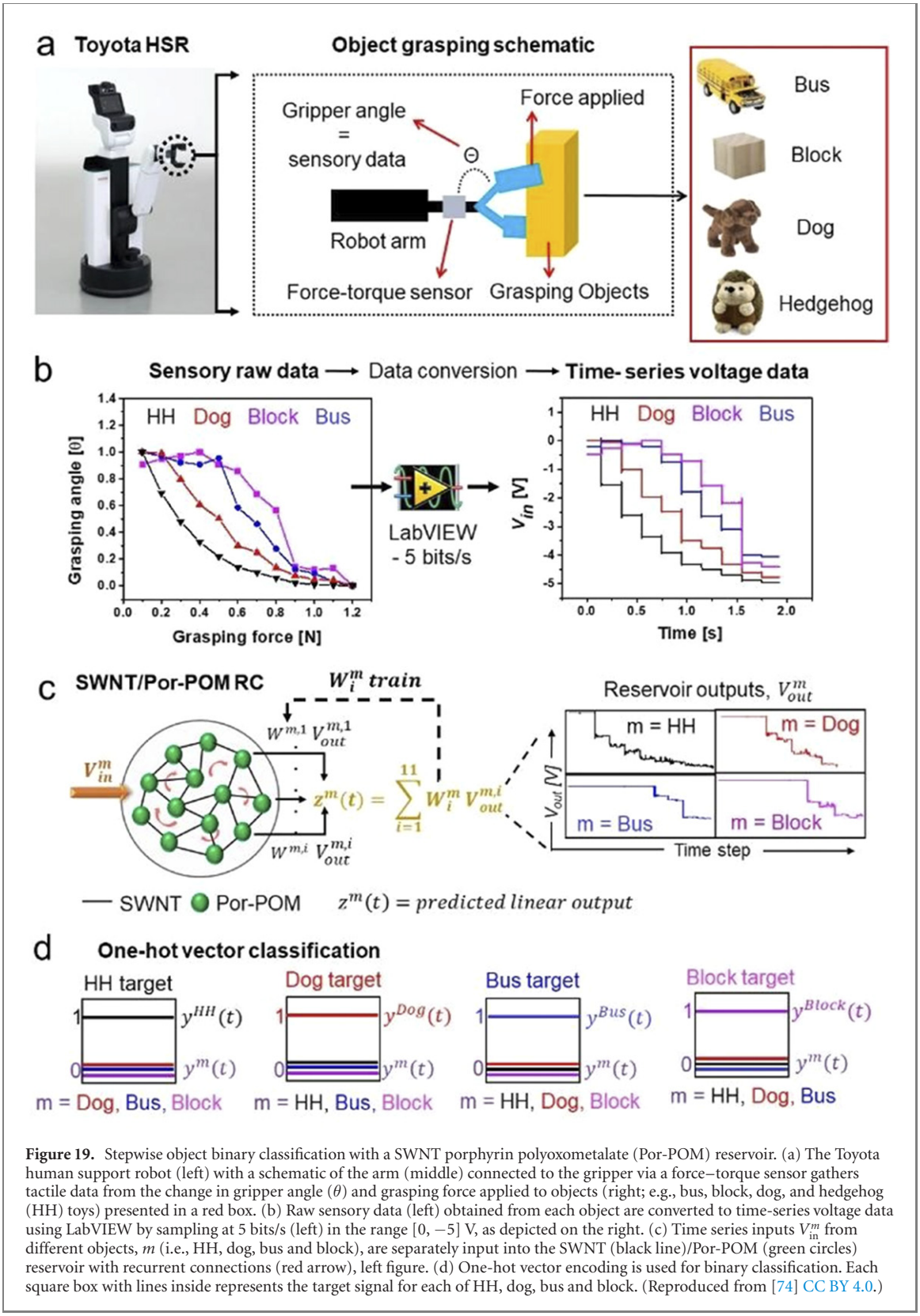

Figure 19. Stepwise object binary classification with a SWNT porphyrin polyoxometalate (Por-POM) reservoir. (a) The Toyota human support robot (left) with a schematic of the arm (middle) connected to the gripper via a force–torque sensor gathers tactile data from the change in gripper angle (θ) and grasping force applied to objects (right; e.g., bus, block, dog, and hedgehog (HH) toys) presented in a red box. (b) Raw sensory data (left) obtained from each object are converted to time-series voltage data using LabVIEW by sampling at 5 bits/s (left) in the range [0, −5] V, as depicted on the right. (c) Time series inputs V_{in}^m from different objects, m (i.e., HH, dog, bus and block), are separately input into the SWNT (black line)/Por-POM (green circles) reservoir with recurrent connections (red arrow), left figure. (d) One-hot vector encoding is used for binary classification. Each square box with lines inside represents the target signal for each of HH, dog, bus and block. (Reproduced from [74] CC BY 4.0.)

To demonstrate performance, the same device was used to apply the RC tasks of NARMA-10, waveform generation, and memory capacity. The results highlight the versatility of the device for RC benchmark performance by controlling and optimizing the voltage outputs with varying degrees of SWNT/PBMA concentration [60]. OR and AND Boolean logic gates and a half-adder operation were also accommodated by varying SWNT concentrations. The upper limit of the linear increase in viscosity and conductivity against the concentration of SWNTs of approximately 1% showed the best operational performance [70]. A simulation attempt was made to solve the traveling salesman problem [71, 72], where Pi-swarm robots were tasked with moving along a maze to reach an end goal without colliding [73].

In another report, it was shown that a physical RC platform consisting of a recurrent SWNT-porphyrin polyoxometalate complex network successfully executed fundamental reservoir properties of nonlinearity, higher harmonic generation, and $1/f\gamma$ power-law information processing [9, 74, 75], where $1/f\gamma$ implies a scale-free network distribution with self-organized criticality analogues to the human brain. A one-hot vector target-based supervised object classification task using tactile input [74], performed by a Toyota human support robot [76], was executed by following a known Robo Cup worldwide [77] task. This was the first report of an RC device consisting of a CNT RNW reservoir device directly induced in a robot for a recognition task (figure 19).

A room-temperature demonstration of an *in-materio* RC with the same material was performed [78] in which Boolean OR, AND, NOR, NAND, XOR, and XNOR functions were reconstructed with an >90% accuracy via the supervised training of linear voltage readouts. The RC prerequisite of an echo-state property and a recurrent connection enabled consistent performance over multiple test datasets and time-shifted target sequences.

We expect that an *in-materio* AI system fabricated using material hardware will be realized in the next generation of computing devices.

5. Conclusion

In this article, we surveyed the historic results of initial CNT electrical measurement, the electrical nonlinearity of individual CNTs, and those complexed with molecules, neuromorphic devices, and hardware used for RNWs of CNTs and RC devices. We recounted the processes by which CNT RNWs obtain intelligence so that they can be used for *in-materio* computing. The surveyed studies demonstrate the potential of CNTs and their complexes as candidates for future AI computing and robotics. Of course, much work is still needed before such devices can become commercialized, but the path is clearing daily. Moreover, *in-materio* computing is not necessarily bound to CNTs; many other media are being investigated. We leave the review of other *in-materio* compounds for RC capabilities to others. In the meantime, this review clearly demonstrates how material engineering can play a role in the development of low-energy AI systems.

Acknowledgments

This review article was partially related to the activity in projects conducted by JSPS KAKENHI (Grant Nos. 19K22114, 19H02559, 20K21819, and 22H01900), JSPS and JST CREST (Grant No. JPMJCR21B5). SA and YU thank Asahi Kosan Co., Ltd. for budget support through the Kitakyushu Foundation for the Advancement of Industry, Science, and Technology, Japan.

Data availability statement

No new data were created or analysed in this study.

ORCID iDs

H Tanaka https://orcid.org/0000-0002-4378-5747
S Azhari https://orcid.org/0000-0002-7043-0909
Y Usami https://orcid.org/0000-0002-8583-325X

References

[1] Indiveri G *et al* 2011 Neuromorphic silicon neuron circuits *Front. Neurosci.* **5** 73
[2] Tanaka G, Nakane R, Yamane T, Takeda S, Nakano D, Nakagawa S and Hirose A 2017 Waveform classification by memristive reservoir computing *Int. Conf. Neural Information Processing* (Lecture Notes in Computer Science vol 10637) pp 457–65
[3] Dale M, Evans R F L, Jenkins S, O'Keefe S, Sebald A, Stepney S, Torre F and Trefzer M 2021 Reservoir computing with thin-film ferromagnetic devices (arXiv:2101.12700)
[4] Jiang W, Chen L, Zhou K, Li L, Fu Q, Du Y and Liu R 2019 Physical reservoir computing built by spintronic devices for temporal information processing (arXiv:1901.07879)
[5] Ielmini D and Ambrogio S 2020 Emerging neuromorphic devices *Nanotechnology* **31** 092001
[6] Sung C, Hwang H and Yoo I K 2018 Perspective: a review on memristive hardware for neuromorphic computation *J. Appl. Phys.* **124** 151903
[7] Qin S *et al* 2017 A light-stimulated synaptic device based on graphene hybrid phototransistor *2D Mater.* **4** 035002

[8] Kuncic Z and Nakayama T 2021 Neuromorphic nanowire networks: principles, progress and future prospects for neuro-inspired information processing *Adv. Phys.:* X **6** 1894234
[9] Le Van Quyen M, Chavez M, Rudrauf D and Martinerie J 2003 Exploring the nonlinear dynamics of the brain *J. Physiol. Paris* **97** 629–39
[10] McKenna T M, McMullen T A and Shlesinger M F 1994 The brain as a dynamic physical system *Neuroscience* **60** 587–605
[11] Wright J J and Liley D T J 1996 Dynamics of the brain at global and microscopic scales: neural networks and the EEG *Behav. Brain Sci.* **19** 285–95
[12] Collins P G, Zettl A, Bando H, Thess A and Smalley R E 1997 Nanotube nanodevice *Science* **278** 100–2
[13] Ebbesen T W, Lezec H J, Hiura H, Bennett J W, Ghaemi H F and Thio T 1996 Electrical conductivity of individual carbon nanotubes *Nature* **382** 54–6
[14] Tans S J, Verschueren A R M and Dekker C 1998 Room-temperature transistor based on a single carbon nanotube *Nature* **393** 49–52
[15] Pang C-S, Han S-J and Chen Z 2021 Steep slope carbon nanotube tunneling field-effect transistor *Carbon* **180** 237–43
[16] Yousefi A T, Fukumori M, Raj P R, Liu P, Fu L, Bagheri S and Tanaka H 2016 Progress on nanoparticle-based carbon nanotube complex: fabrication and potential application *Rev. Inorg. Chem.* **36** 183–201
[17] Tanaka H, Yajima T, Matsumoto T, Otsuka Y and Ogawa T 2006 Porphyrin molecular nanodevices wired using single-walled carbon nanotubes *Adv. Mater.* **18** 1411–5
[18] Setiadi A *et al* 2017 *Nanoscale* **9** 10674–83
[19] Tanaka H, Yajima T, Kawao M and Ogawa T 2006 Electronic properties of a single-walled carbon nanotube/150mer-porphyrin system measured by point-contact current imaging atomic force microscopy *J. Nanosci. Nanotechnol.* **6** 1644–8
[20] Subramaniam C *et al* 2007 Visible fluorescence induced by the metal semiconductor transition in composites of carbon nanotubes with noble metal nanoparticles *Phys. Rev. Lett.* **99** 167404
[21] Hong L, Tanaka H and Ogawa T 2013 Rectification direction inversion in a phosphododecamolybdic acid/single-walled carbon nanotube junction *J. Mater. Chem.* C **1** 1137–43
[22] Yu W J, Kim U J, Kang B R, Lee I H, Lee E-H and Lee Y H 2009 Adaptive logic circuits with doping-free ambipolar carbon nanotube transistors *Nano Lett.* **9** 1401–5
[23] Geier M L, Prabhumirashi P L, McMorrow J J, Xu W, Seo J-W T, Everaerts K, Kim C H, Marks T J and Hersam M C 2013 Subnanowatt carbon nanotube complementary logic enabled by threshold voltage control *Nano Lett.* **13** 4810–4
[24] Gowda P, Suri A, Reddy S K and Misra A 2014 Chemical vapor detection using nonlinear electrical properties of carbon nanotube bundles *Nanotechnology* **25** 025708
[25] Liu X *et al* 2016 A p–i–n junction diode based on locally doped carbon nanotube network *Sci. Rep.* **6** 23319
[26] Chen C *et al* 2016 Carbon nanotube intramolecular p–i–n junction diodes with symmetric and asymmetric contacts *Sci. Rep.* **6** 22203
[27] Gao X, Du X, Mathis T S, Zhang M, Wang X, Shui J, Gogotsi Y and Xu M 2020 Maximizing ion accessibility in MXene-knotted carbon nanotube composite electrodes for high-rate electrochemical energy storage *Nat. Commun.* **11** 6160
[28] Valentini L, Bon S B, Signetti S, Tripathi M, Iacob E and Pugno N M 2016 Fermentation based carbon nanotube multifunctional bionic composites *Sci. Rep.* **6** 27031
[29] Tanaka H *et al* 2018 A molecular neuromorphic network device consisting of single-walled carbon nanotubes complexed with polyoxometalate *Nat. Commun.* **9** 2693
[30] Zhao W S, Agnus G, Derycke V, Filoramo A, Bourgoin J P and Gamrat C 2010 Nanotube devices based crossbar architecture: toward neuromorphic computing *Nanotechnology* **21** 175202
[31] Kim K, Chen C-L, Truong Q, Shen A M and Chen Y 2013 A carbon nanotube synapse with dynamic logic and learning *Adv. Mater.* **25** 1693–8
[32] Shen A M, Chen C-L, Kim K, Cho B, Tudor A and Chen Y 2013 Analog neuromorphic module based on carbon nanotube synapses *ACS Nano* **7** 6117–22
[33] Shen A M, Kim K, Tudor A, Lee D and Chen Y 2015 Doping modulated carbon nanotube synapstors for a spike neuromorphic module *Small* **11** 1571–9
[34] Li M, Xiong Z, Shao S, Shao L, Han S-T, Wang H and Zhao J 2021 Multimodal optoelectronic neuromorphic electronics based on lead-free perovskite-mixed carbon nanotubes *Carbon* **176** 592–601
[35] Shao L *et al* 2019 Optoelectronic properties of printed photogating carbon nanotube thin film transistors and their application for light-stimulated neuromorphic devices *ACS Appl. Mater. Interfaces* **11** 12161–9
[36] Wang Y, Huang W, Zhang Z, Fan L, Huang Q, Wang J, Zhang Y and Zhang M 2021 Ultralow-power flexible transparent carbon nanotube synaptic transistors for emotional memory *Nanoscale* **13** 11360–9
[37] Li M *et al* 2021 Flexible printed single-walled carbon nanotubes olfactory synaptic transistors with crosslinked poly(4-vinylphenol) as dielectrics *Flexible Printed Electron.* **6** 034001
[38] Kim S, Lee Y, Kim H-D and Choi S-J 2020 A tactile sensor system with sensory neurons and a perceptual synaptic network based on semivolatile carbon nanotube transistors *NPG Asia Mater.* **12** 76
[39] Ou Q, Yang B, Zhang J, Liu D, Chen T, Wang X, Hao D, Lu Y and Huang J 2021 Degradable photonic synaptic transistors based on natural biomaterials and carbon nanotubes *Small* **17** 2007241
[40] Lecun Y, Bengio Y and Hinton G 2015 Deep learning *Nature* **521** 436–44
[41] Li J, Deng L, Haeb-Umbach R and Gong Y 2015 *Robust Automatic Speech Recognition: A Bridge to Practical Applications* (New York: Academic)
[42] Graves A, Liwicki M, Fernandez S, Bertolami R, Bunke H and Schmidhuber J 2008 A novel connectionist system for improved unconstrained handwriting recognition *IEEE Trans. Pattern Anal. Mach. Intell.* **31** 855–68
[43] Sak H, Senior A W and Beaufays F 2014 Long short-term memory recurrent neural network architectures for large scale acoustic modeling pp 338–42 *Proc. INTERSPEECH*
[44] Li X and Wu X 2015 Constructing long short-term memory based deep recurrent neural networks for large vocabulary speech recognition *2015 IEEE Int. Conf. Acoustics, Speech and Signal Processing (ICASSP)*
[45] Jaeger H 2001 The 'echo state' approach to analysing and training recurrent neural networks-with an erratum note 148 (German National Research Center for Information Technology)
[46] Jaeger H and Haas H 2004 Harnessing nonlinearity: predicting chaotic systems and saving energy in wireless communication *Science* **304** 78–80

[47] Maass W, Natschläger T and Markram H 2002 Real-time computing without stable states: a new framework for neural computation based on perturbations *Neural Comput.* **14** 2531–60
[48] Lukoševičius M and Jaeger H 2009 Reservoir computing approaches to recurrent neural network training *Comput. Sci. Rev.* **3** 127–49
[49] Verstraeten D, Schrauwen B, D'Haene M and Stroobandt D 2007 An experimental unification of reservoir computing methods *Neural Netw.* **20** 391–403
[50] Schuman C D *et al* 2017 A survey of neuromorphic computing and neural networks in hardware (arXiv:1705.06963)
[51] Lukoševičius M, Jaeger H and Schrauwen B Reservoir computing trends 2012 *Künstl. Intell.* **26** 365–71
[52] Goudarzi A, Lakin M R and Stefanovic D 2014 Reservoir computing approach to robust computation using unreliable nanoscale networks *The Int. Conf. on Unconventional Computation and Natural Computation (UCNC 2014)* pp 164–76
[53] Tanaka G, Yamane T, Héroux J B, Nakane R, Kanazawa N, Takeda S, Numata H, Nakano D and Hirose A 2019 Recent advances in physical reservoir computing: a review *Neural Netw.* **115** 100–23
[54] Nakajima K 2020 Physical reservoir computing-an introductory perspective *Japan. J. Appl. Phys.* **59** 060501
[55] Sillin H O, Aguilera R, Shieh H-H, Avizienis A V, Aono M, Stieg A Z and Gimzewski J K 2013 A theoretical and experimental study of neuromorphic atomic switch networks for reservoir computing *Nanotechnology* **24** 384004
[56] Kotooka T *et al* 2021 Ag_2Se nanowire network as an effective *in-materio* reservoir computing device *arXiv Preprint* https://doi.org/10.1016/C2009-0-25523-1(Nature Portfolio)
[57] Hadiyawarman , Usami Y, Kotooka T, Azhari S, Eguchi M and Tanaka H 2021 Performance of Ag–Ag_2S core-shell nanoparticle-based random network reservoir computing device *Japan. J. Appl. Phys.* **60** SCCF02
[58] Milano G, Pedretti G, Montano K, Ricci S, Hashemkhani S, Boarino L, Ielmini D and Ricciardi C 2022 In materia reservoir computing with a fully memristive architecture based on self-organizing nanowire networks *Nat. Mater.* **21** 195–202
[59] Mohid M, Miller J F, Harding S L, Tufte G, Massey M K and Petty M C 2016 Evolution-*in-materio*: solving computational problems using carbon nanotube–polymer composites *Soft Comput.* **20** 3007–22
[60] Dale M, Miller J F, Stepney S and Trefzer M A 2016 Evolving carbon nanotube reservoir computers *Int. Conf.Unconventional Computation and Natural Computation* (Lecture Notes in Computer Science vol 9726) pp 49–61
[61] Usami Y *et al* 2021 *In-materio* reservoir computing in a sulfonated polyaniline network *Adv. Mater.* **33** 2102688
[62] Duport F, Smerieri A, Akrout A, Haelterman M and Massar S 2014 Virtual optical reservoir computing *Spec. Opt. Fibers SOF* vol 20 pp 1958–64
[63] Paquot Y *et al* 2012 Optoelectronic reservoir computing *Sci. Rep.* **2** 287
[64] Nakajima K, Hauser H, Li T and Pfeifer R 2015 Information processing via physical soft body *Sci. Rep.* **5** 10487
[65] Nakajima K, Hauser H, Kang R, Guglielmino E, Caldwell D G and Pfeifer R 2013 A soft body as a reservoir: case studies in a dynamic model of octopus-inspired soft robotic arm *Front. Comput. Neurosci.* **7** 91
[66] Torrejon J *et al* 2017 Neuromorphic computing with nanoscale spintronic oscillators *Nature* **547** 428–31
[67] Fernando C and Sojakka S 2003 Pattern recognition in a bucket *European Conf. Artificial Life* (Lecture Notes in Computer Science vol 2801) pp 588–97
[68] Akai-Kasaya M, Takeshima Y, Kan S, Nakajima K, Oya T and Asai T 2022 Performance of reservoir computing in a random network of single-walled carbon nanotubes complexed with polyoxometalate *Neuromorph. Comput. Eng.* **2** 014003
[69] Wu S, Zhou W, Wen K, Li C and Gong Q 2021 Improved reservoir computing by carbon nanotube network with polyoxometalate decoration *2021 IEEE 16th Int. Conf. Nano/Micro Engineered and Molecular Systems (NEMS)* pp 994–7
[70] Lykkebø O R, Harding S, Tufte G and Miller J F 2014 Mecobo: a hardware and software platform for *in-materio* evolution *Unconventional Computation and Natural Computation* pp 267–79
[71] Massey M K, Kotsialos A, Qaiser F, Zeze D A, Pearson C, Volpati D, Bowen L and Petty M C 2015 Computing with carbon nanotubes: optimization of threshold logic gates using disordered nanotube/polymer composites *J. Appl. Phys.* **117** 134903
[72] Clegg K D, Miller J F, Massey M K and Petty M C 2014 Practical issues for configuring carbon nanotube composite materials for computation *2014 IEEE Int. Conf. Evolvable Systems* pp 61–8
[73] Mohid M and Miller J F 2015 Evolving robot controllers using carbon nanotubes *European Conf. Artificial Life* vol 1998 pp 106–13
[74] Banerjee D, Kotooka T, Azhari S, Usami Y, Ogawa T, Gimzewski J K, Tamukoh H and Tanaka H 2022 Emergence of *in-materio* intelligence from an incidental structure of a single-walled carbon nanotube-porphyrin polyoxometalate random network *Adv. Intell. Syst.* **4** 2100145
[75] Hochstetter J, Zhu R, Loeffler A, Diaz-Alvarez A, Nakayama T and Kuncic Z 2021 Avalanches and edge-of-chaos learning in neuromorphic nanowire networks *Nat. Commun.* **12** 4008
[76] Toyota Motor Corporation 2015 Toyota shifts home helper robot R & D into high gear with new developer community and upgraded prototype https://global.toyota/en/detail/8709541 (accessed 16 July 2015)
[77] RoboCup Federation RoboCup Federation official website https://robocup.org/
[78] Banerjee D, Azhari S, Usami Y and Tanaka H 2021 Room temperature demonstration of *in-materio* reservoir computing for optimizing Boolean function with single-walled carbon nanotube/porphyrin-polyoxometalate composite *Appl. Phys. Express* **14** 105003